East European Journal of Physics. 1. 109-117 (2023)
DOI:10.26565/2312-4334-2023-1-13 ISSN 2312-4334

THE ELECTRONIC AND THERMODYNAMIC PROPERTIES OF TERNARY RARE EARTH METAL ALLOYS†

Aman Kumar[a,*], Anuj Kumar[b], Kamal Kumar[c], Rishi Pal Singh[d], Ritu Singh[e], Rajesh Kumar[f]

[a]*Department of Physics, Keral Verma Subharti College of Science, Swami Vivekanand Subharti University Meerut, Uttar Pradesh, India*
[b]*Department of Physics, Mahamaya Government Degree College, Sherkot, Bijnore, Uttar Pradesh, India*
[c]*Department of Physics, D.A.V College Kanpur, Uttar Pradesh, India*
[d]*Department of Physics, S. S. V. College, Hapur 245101, Uttar Pradesh, India*
[e]*Department of Chemistry, S. S. V. College, Hapur 245101, Uttar Pradesh, India*
[f]*Department of Physics, Government Degree College, Nanauta, Saharanpur, UP, Pin-247452, India*
**Corresponding Author e-mail: 01amankumar@gmail.com*
Received January 3, 2023; revised January 29, 2023; accepted January 30, 2023

This article uses the FP-LAPW approach within the DFT method, and the quasi-harmonic Debye model to investigate the electronic and thermodynamic properties of intermetallic rare earth materials (such as SmInZn, SmInCd, and SmTlZn). Thermodynamic properties were determined by the quasi-harmonic Debye model, whereas the FP-LAPW approaches within DFT method were utilized to derive electronic properties. The calculated structural parameters and the available experimental data have been examined, and it was observed that there was a good agreement between available experimental and calculated values of structural parameters. The electronic behavior of SmInZn, SmInCd and SmTlZn compounds shows the metallic character. We have examined a few thermodynamic characteristics. All calculated characteristics were found to match experimental or theoretical calculations.
Keywords: *electronic; intermetallic; density of state; DFT*
PACS: 71.20.Lp; 71.20.Eh 71.20._b

INTRODUCTION

A lot of investigation has been done on the equal-atomic ternary rare-earth intermetallic compounds, owing to their various interesting properties in the field of material science. In recent years, intermetallic compounds have received a lot of attention from scientists due to their distinctive properties. They exhibit numerous structural properties [1-2]. There is a focus on structural, electronic, magnetic, and thermodynamic properties, such as fermionic, heavy-fermions [3-4], and half-metallic behavior in rare-earth intermetallic compounds such as SmInZn, SmInCd and SmTlZn [5–6], and the giant magneto-resistance device is an industrial application of heavy rare earth compounds [7-9]. These equal-atomic type compounds of rare earth have been investigated seriously in the last few years [10-15]. Sm-based compounds have been studied with theoretical and experimental significance [16-20]. It is seen from this study that Sm-based compounds can be used for refrigeration. This is based on the magneto-caloric effect (MCE) [21]. The SmInZn, SmInCd and SmTlZn compounds show many interesting applications in spintronics devices, magnetic sensors, unconventional superconductors, met-magnetism, magnetic random-access memories, and spin glass [21-22]. In this calculation, we used the space group P63/mmc (number-194) for the SmInZn, SmInCd and SmTlZn rare-earth compounds, and their crystal structures are similar to those of $CaIn_2$ at low temperatures [21].

Table 1. SmInZn, SmInCd and SmTlZn crystallographic data (space group and Wyckoff position).

Compound	Space group	Atoms	X	Y	z
SmInZn, SmInCd SmTlZn	P63/mmc (194)	Sm	0	0	0
		In/Tl	1/3	2/3	1/4
		Zn/Cd	1/3	2/3	3/4

The calculations have been executed with the help of the first principle method based on DFT, which is exerted in WIEN2K software package [23]. We have investigated the electronic and thermodynamic characteristics of SmInZn, SmInCd, and SmTlZn compounds using the FP-LAPW technique and GGA approximation [24, 25]. Here, structural and electronic properties are described, such as the energy Vs volume curve (which shows the stability of material), band diagrams, and, total and partial density of states. Thermodynamic behaviors of the SmInZn, SmInCd and SmTlZn compounds have been investigated with the help of GIBBS2 software. It's based on the Quasi Harmonic Debye (QHD) model [26]. In thermodynamics behavior, we have investigated some parameter like bulk modulus of materials (B_0), specific heat (Cv), Grüneisen parameter (γ), Debye temperature (θ_D), thermal expansion coefficient (α) and entropy (S).

COMPUTATIONAL METHOD

This article has been presented for first-principal calculations using full-potential approach based on DFT, it is utilized by the software WIEN2K [27-28], to investigate the electronic and thermodynamic properties of SmInZn,

† ***Cite as:*** A. Kumar, A. Kumar, K. Kumar, R.P. Singh, R. Singh, and R. Kumar, East Eur. J. Phys. **1**, 109 (2023), https://doi.org/10.26565/2312-4334-2023-1-13

SmInCd, and SmTlZn. In this modern DFT approach method; exchange-correlation energy potential has played an important role in the SCF process based on GGA [29]. In the SCF process, we take the value of cut-off parameter Kmax = $7/R_{MT}$ [where Kmax is the magnitude of largest reciprocal lattice vector and R_{MT} is the minimum radii of atoms in BZ (Brillouin zone)] and R_{MT} values have been taken 2.50 a.u. for Gd and Sb atoms and 2.46 a.u. for Ni atom. In SCF process, 47 k-mess points and 2000 k-point was used in the irreducible parts of full BZ and cut-off energy −6.0 Ry. We have chosen the energy convergence 0.0001ec. The energy terms used in this process gives information about valence and core atomic states. The total energy Vs volume curve has been fitted in the Brich-Murnaghan equation of state (EOS) [30]. Thermodynamics behaviors of the SmInZn, SmInCd and SmTlZn compound have been investigated, with the help of GIBBS2 software. It's based on the Quasi Harmonic Debye (QHD) model.

RESULTS

Structural and electronic properties

The stability curves (volume vs energy curve) can be used to calculate the structural characteristics of an intermetallic compound. The bulk modulus of material (B_0), pressure derivative bulk modulus of material (B_0'), and lattice constant (a_0) parameters were derived from structural characteristics. Figures 1(a), 1(b), and 1(c) depict the energy vs. volume curve (i.e., material stability curve) for SmInZn, SmInCd, and SmTlZn respectively, as fitted by the Brich-Murnaghan equation of state (EOS).

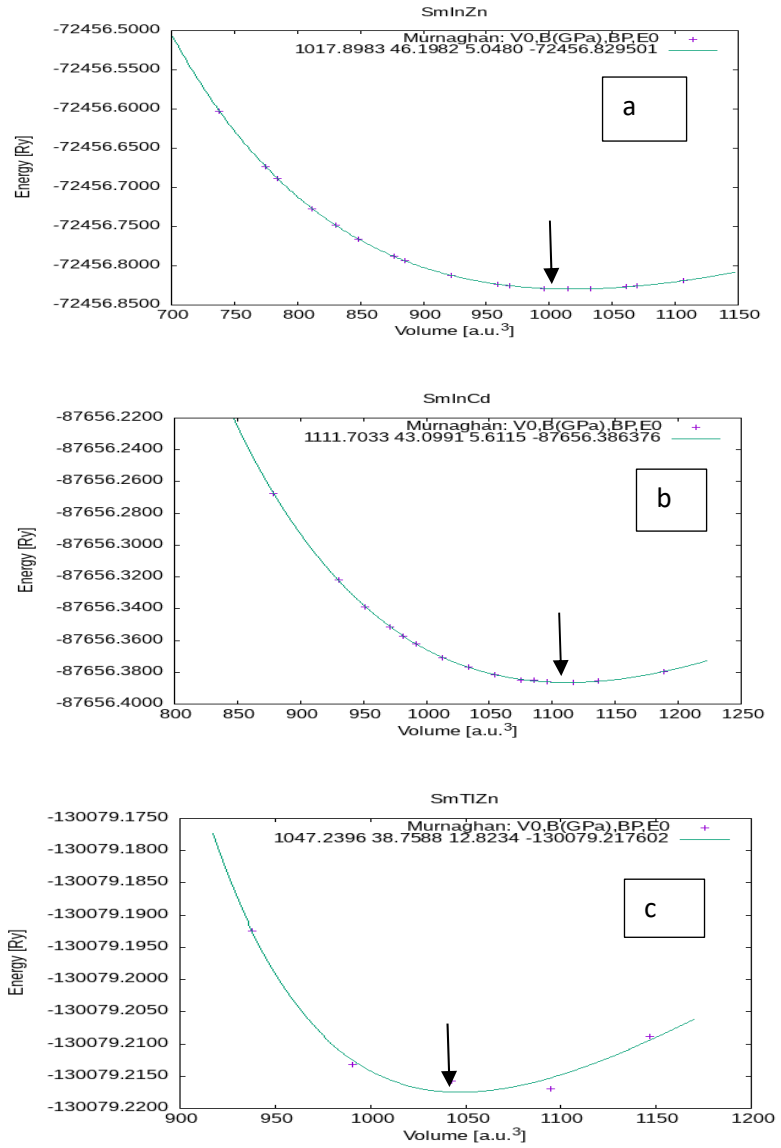

Fig. 1 Total energy Vs unit cell volume for (a) SmInZn (b) SmInCd and (c) SmTlZn

Using the optimization method and revealing that compound SmInZn is stable with a minimum energy value (E_0 = -72456.829501 Ry) at the minimum volume (V_0 = 1017.8983 a. u^3). The optimization method revealed that compound SmInCd is stable with a minimum energy value (E_0 = -87656.386376 Ry) at the minimum volume (V_0 = 1111.7033 a. u^3) while SmTlZn is stable with a minimum energy value (E_0 = -130079.217602 Ry) at the minimum

volume (V_0 = 1047.2396 a. u^3). After calculating the energy Vs. volume curve (i.e., material stability curve), we get the values of lattice constant (a_0), bulk modulus of material (Bo) and pressure derivative of bulk modulus of material (B_0'). (See Table 2). These structural parameters are obtained using the GGA approximation. The value of the lattice constant we determined from our calculations is supported by some research on these compounds [32].

Table 2. Some structural parameters calculated using the GGA approximation

Parameter	Symbols	SmInZn	SmInCd	SmTlZn
Lattice parameters (Å)	a_0	4.0952	4.8660	4.7780
	c_0	6.5879	7.4690	7.8130
Bulk modulus of material (GPa)	B_0	46.1982	43.0991	38.7588
Pressure derivative of bulk modulus of material (GPa)	B_0'	5.0480	5.6115	12.8234
Energy at equilibrium Condition (Ryd.)	E_{min}	-72456.829501	-87656.386376	-130079.217602
Volume of Unit cell at equilibrium condition (a. u. ^3)	V_0	1017.8983	1111.7033	1047.2396

At present, we are discussing here spin polarized electronic characteristics such as energy bands and DOS (i.e., density of states). The calculated energy bands for majority and minority spin channels along the high symmetry directions Γ, Σ, M, K, Λ and Δ in the first Brillouin zone for SmInZn, SmInCd, and SmTlZn compounds were obtained using GGA approaches, which are shown in Figures 2 (a) to 2 (f) respectively. Figures 2(a) and 2(b) show band structures for spin up and spin down for SmInZn Compound. Similarly, Figs. 2(c) and 2(d) have been represented for SmInCd, and Figs. 2(e) and 2(f) have been depicted for SmTlZn compound.

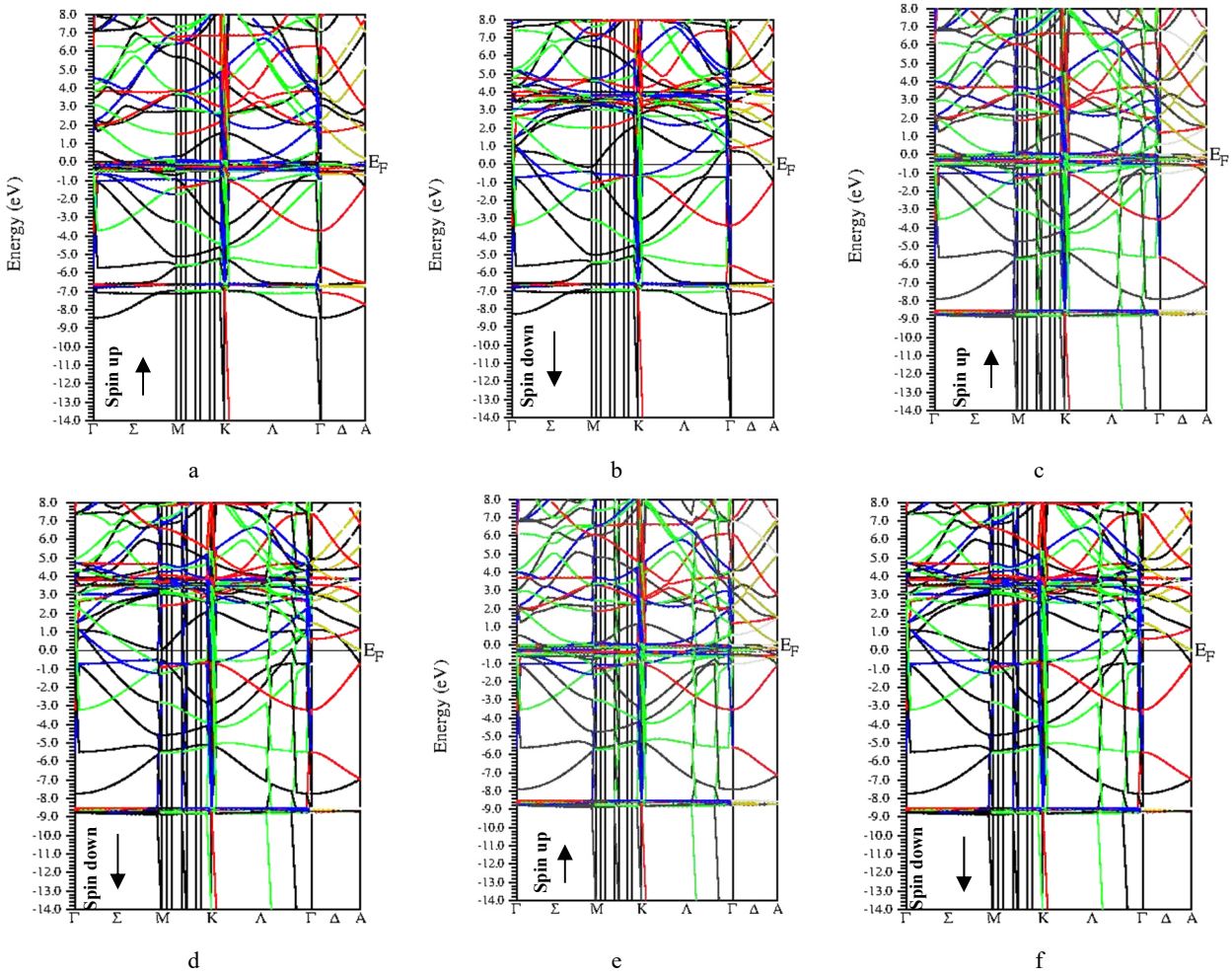

Figure 2. Band diagram for (a) spin up for SmInZn (b) spin down for SmInZn (c) spin up for SmInCd (d) spin down for SmInCd (e) spin up for SmTlZn (f) spin down for SmTlZn

It is clear from these graphs that most of the energy levels in the valence bands lie between -8.0 eV and 0.0 eV and conduction bands lies above 0.0 eV, Whereas the Fermi level is assumed to at the origin. It can be seen from Figure 2(a,b,c,d,e,f) Due to the electronic arrangement of Tl and In [Xe] $4f^{14}5d^{10}6s^26p$ and [Kr] $4d^{10}5S^25p^1$, the bands that were present in at roughly-09.0 eV in SmTlZn, SmInZn and SmInCd for spin up have been disappear in spin down bands, as can be seen in Figs. 2(a)–(f) (i.e. these bands in exist due to Zn bands).

Additionally, the valence band and conduction bands both cross the Fermi level, so there is no band gap. Thus, three compounds (SmInZn, SmInCd, and SmTlZn) indicative metallic properties. The Sm-f orbitals are mainly to blame for the formation of these bands. Now we are going to talk about the total densities of states, also known as T-DOS, for providing metallic character to these compounds. In addition, the profile of the partial densities of states (P-DOS) for the SmInZn, SmInCd, and SmTlZn compounds have been calculated with the help of the GGA approach and are plotted in graphs in Figure 3 (a-i) for SmInZn, Figure 4 (a-i) for SmInCd, and Figure 5 (a-i) for SmTlZn.

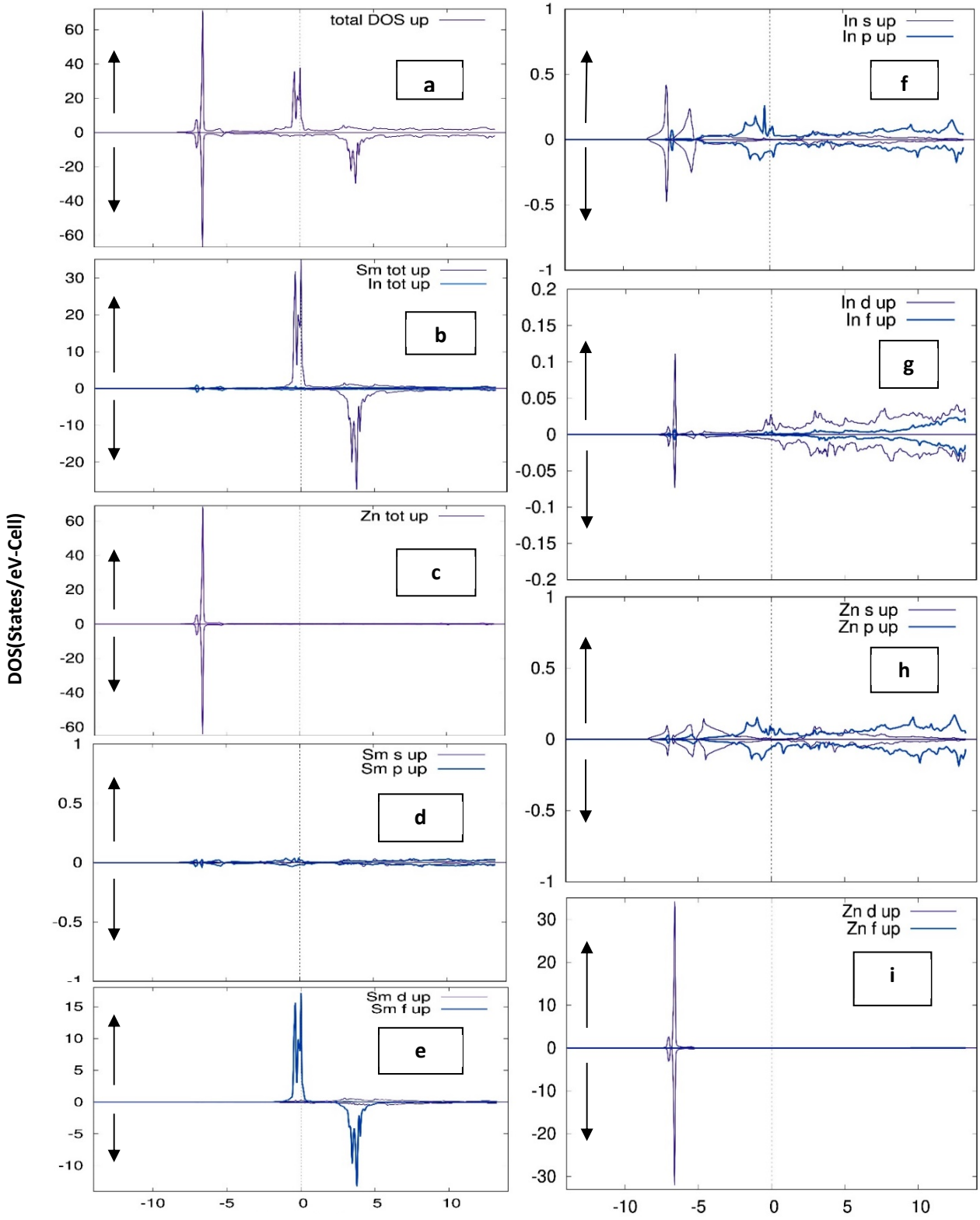

Figure 3. T-DOS and P-DOS for (a) SmInZn -Total (b) Sm-Total & In-Total (c) Zn-Total (d) Sm-s & Sm-p (e) Sm-d & Sm-f (f) In-s & In-p (g) In-d & In-f (h) Zn-s & Zn-p (i) Zn-d & Zn-f

The Fermi level at the origin can be seen in Fig. 3(a-i). It has been found that three sharp peaks are at around 0, -1 and -7 electron-volts (eV) in the spin-up state below the Fermi level and also one peaks are obtained at around +4 electron-volts(eV) above the Fermi level. It has been found that one sharp peak is at Fermi level in a spin-down state. According to our observations, the Zn-d states are responsible for the peak that occurs at around -7 eV below the Fermi level for both channels. A small contribution of In-s and In-d states. A second peak at about 0 eV and -1 eV is caused by the spin-up state of Sm-f state and a minor contribution from In-d and Zn-p states.

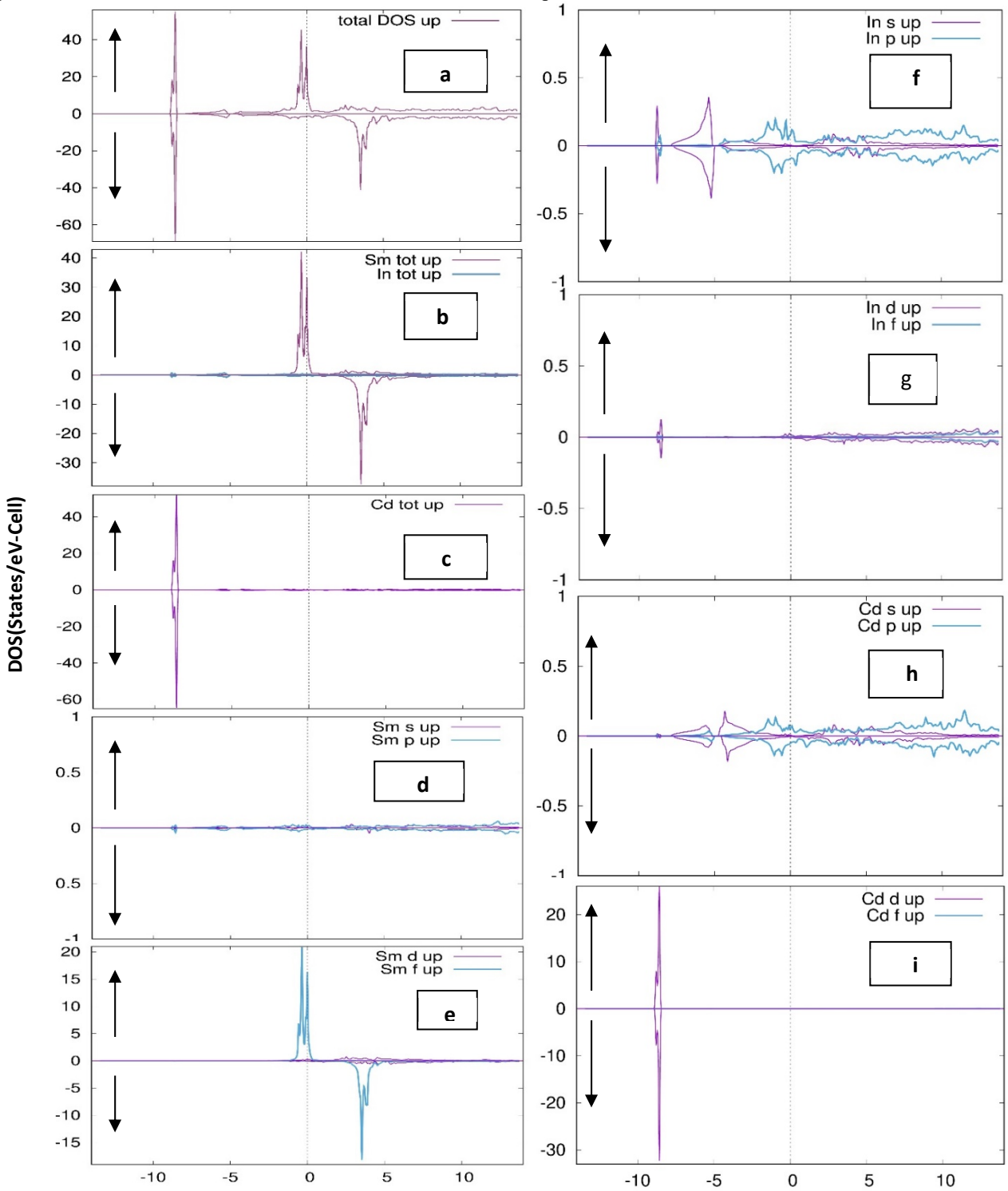

Figure 4. T-DOS and P-DOS for (a) SmInCd -Total (b) Sm-Total & In-Total (c) Cd-Total (d) Sm-s & Sm-p (e) Sm-d & Sm-f (f) In-s & In-p (g) In-d & In-f (h) Cd-s & Cd-p (i) Cd-d & Cd-f.

Now we discuss another peak at around +4e V is caused by spin down state of Sm-f state above the Fermi level. The Fermi level at the origin can be seen in Fig. 4(a-i). It has been found that three sharp peak is at around 0 eV, -1 eV spin up state and -9 electron-volts (eV) in the both state below the Fermi level and also one peak is obtained at around

+4 electron-volts(eV) in the spin down state above the Fermi level. We notice that a sharp peak around -9 eV is caused by the Cd-d states with small contribution In-s and In-d state for both channels. A second peak at about 0 eV and -1 eV is caused by the spin-up state of Sm-f states and a minor contribution from In-p and Cd-p states. Now we discuss another peak at around +4e V is caused by spin down state of Sm-f state above the Fermi level. The Fermi level at the origin can be seen in Fig. 5(a-i).

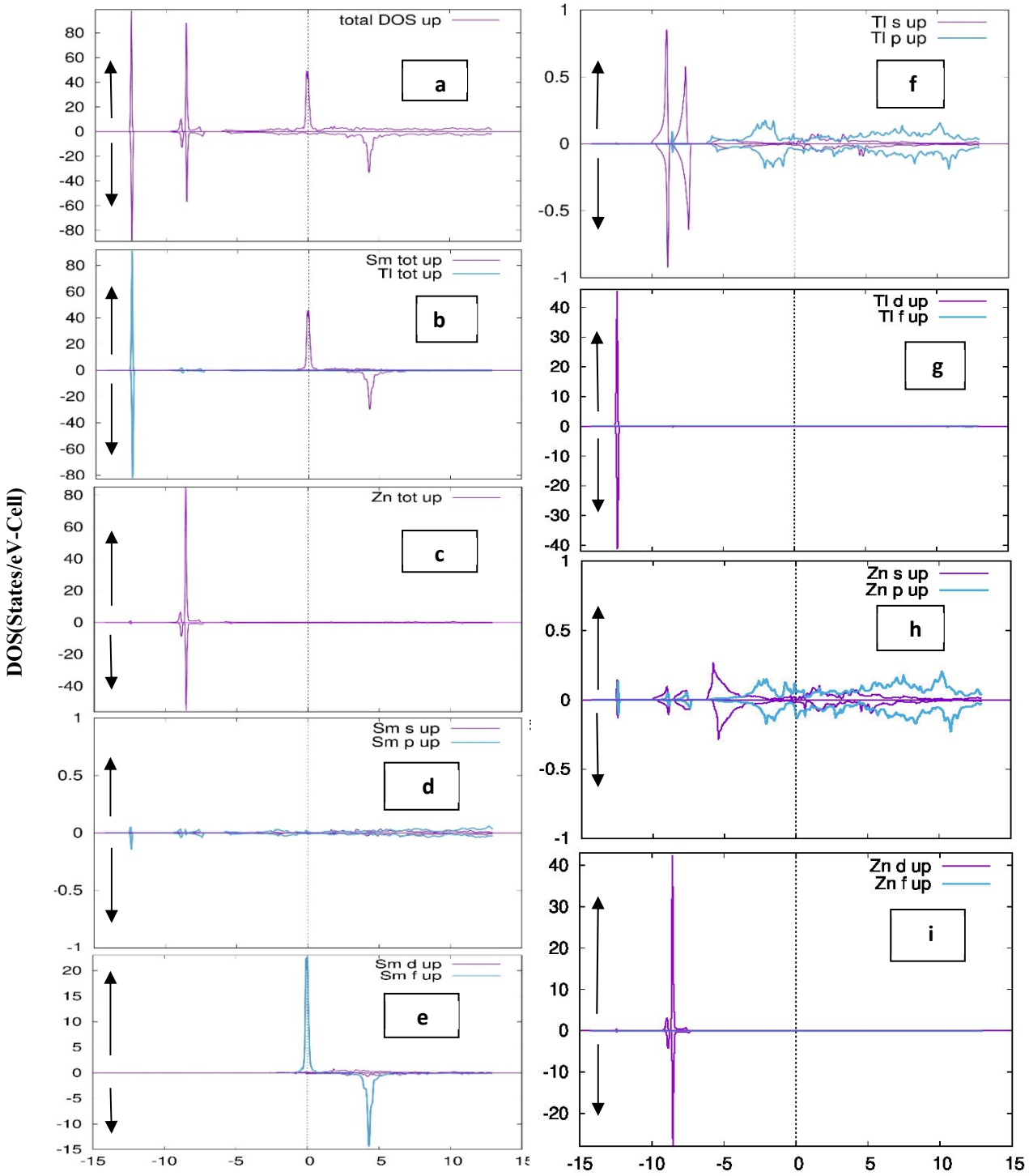

Figure 5. T-DOS and P-DOS for (a) SmTlZn -Total (b) Sm-Total & Tl-Total (c) Zn-Total (d) Sm-s & Sm-p (e) Sm-d & sm-f (f) Tl-s & Tl-p (g) Tl-d & Tl-f (h) Zn-s & Zn-p (i) Zn-d & Zn-f.

It has been found that four sharp peaks are at around -9 eV and -13 electron-volts (eV) in both states below the Fermi level, and also one peak found around 0 eV in the spin up state at Fermi level. And one peak is obtained at around +4 electron-volts (eV) in the spin down state above the Fermi level. We observe that the peak of around -9 eV for both channels below the Fermi level is caused by the Zn-d state with the hybridization of the Zn-s and Tl-s states. Another peak at around -13 eV is caused by the both state of Tl-d states and a minor contribution from Zn-p and Zn-s states. The

peak around 0 eV is caused by spin up state of Sm-f state at Fermi level. Another peak around +4 eV is caused by spin down state of Sm-f state above the Fermi level. Fermi energy has been found that E_F = 0.52524 electron-volts (eV) for SmInZn, E_F = 0.48818 electron-volts (eV) for SmInCd and E_F = 0.54729 electron-volts (eV) for SmTlZn.

Thermodynamics properties

The QHD model, implemented in the Gibbs software package was used to calculate the thermodynamic properties for SmInZn, SmInCd, and SmTlZn compounds within wide range of temperature (0-400 K). Figures 6(a-f) depict temperature dependent thermodynamics characteristics. In thermodynamic properties, we have extracted some important parameters, such as entropy (S), thermal expansion coefficient (α), bulk modulus of material (B), specific heat at constant volume (C_V), and Debye temperature (θ_D). The variation of the bulk modulus with temperature is shown in Fig. 6(a).

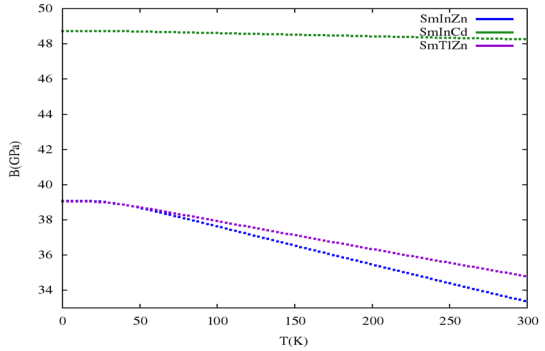

Figure 6(a). Bulk modulus (B) Vs temperature graphs for SmInZn, SmInCd and SmTlZn

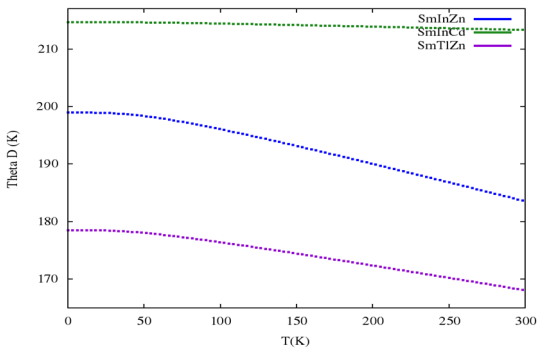

Figure 6(b). Debye temperature (θ_D) Vs temperature graphs for SmInZn, SmInCd and SmTlZn

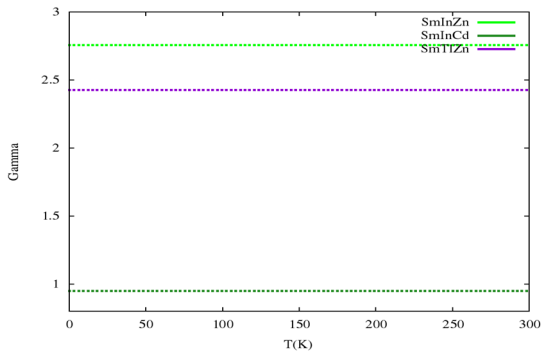

Figure 6(c). Grüneisen parameter (γ) Vs temperature graphs for SmInZn, SmInCd and SmTlZn

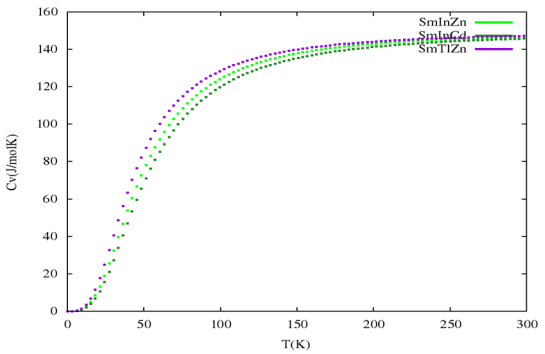

Figure 6(d). Specific heat (C_V) Vs temperature graphs for SmInZn, SmInCd and SmTlZn

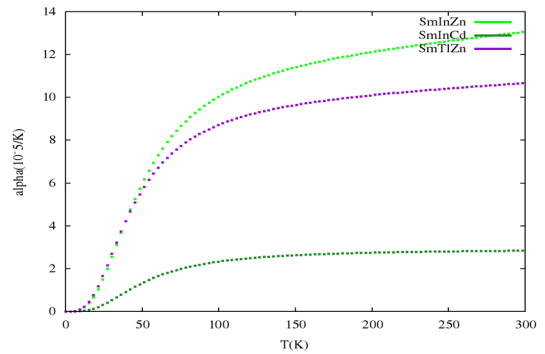

Figure 6(e). Thermal expansion coefficient (α) Vs temperature graphs for SmInZn, SmInCd and SmTlZn

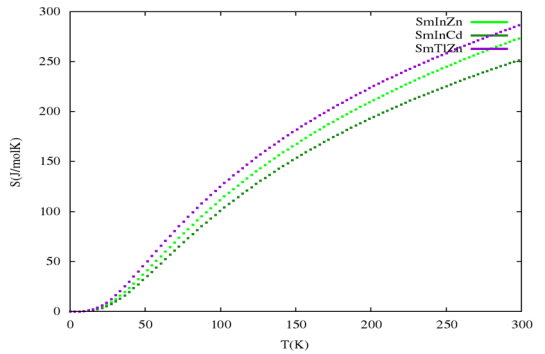

Figure 6(f). Entropy (S) Vs temperature graphs for SmInZn, SmInCd and SmTlZn

These graphs show that as the temperature increases, the bulk modulus (B), decreases. The bulk modulus (B), and compressibility (C), are inversely proportional. So, we can say that as the temperature increases, the compressibility (C), of these compounds will also increase. As a result, Figures 6(a) demonstrates also that as the temperature rises, the three compounds (SmInZn, SmInCd, and SmTlZn) become more compressible, or flexible. Other thermodynamic properties, such as the Debye temperature, provide interesting information about the elastic nature of materials. The relationship between the Debye temperature and temperature is depicted in Figures 6(b), which also demonstrates that for all three compounds.

The Debye temperature (θ_D) gradually decreases as the temperature increases. Additionally, Figs. 6(b) show that SmInZn has a larger θ_D value than SmInCd and SmTlZn, indicating that SmInZn is stiffer than those two metals (as stiff material has a high Debye temperature).

The anharmonicity of crystal lattices under vibrational motion is described by the Grüneisen parameter (γ).

Figures 6(c) indicate how the Grüneisen parameter (γ) changes with temperature and show that it rises with rise in temperature. In the quasi-harmonic Debye model, γ is a function of volume which is depends upon lattice parameters. The dimensions of the lattice and, hence, the volume, grow as the temperature rises so γ also increase with rise in temperature. As a result, increasing temperature raises crystal anharmonicity and the value of γ. A crucial factor that offers crucial insight into the vibrational characteristics and microscopic structure of a crystal is specific heat (C_V).

The variation of specific heat (C_V) is shown in Figures 6 (d) which illustrates how the computed heat capacity at constant volume (C_V) responds to temperature. At temperature ≈ 300 K, it's clear that C_V follows the Debye model relationship (C_V proportional to T^3 law), and beyond T > 300 K, the Dulong-Petit limit is approaching.

The thermal expansion coefficient (α) varies with temperature, as shown in Figures 6(e). it is clear that α increases sharply with temperature when it gets close to 300K. The impact of temperature on the thermal expansion coefficient (α) reduces when temperature rises and exceeding 300 K. when the atoms are moving in a variety of ways. The amount of disorder or irregularity in an atom's or molecule's motion inside a thermodynamic system is described by the entropy(S) Figures 6(f) demonstrate how the entropy (S) for SmInZn, SmInCd, and SmTlZn changes with temperature. Figures 6(f) show that the entropy is zero at absolute zero temperature and that the vibrations inside the thermodynamics system increase as the temperature rises. As a result, the entropy of the system starts to increase rapidly.

CONCLUSIONS

In the current chapter, the DFT approach has been used to examine the electronic properties and quasi-harmonic Debye model has been applied to calculate the thermodynamic characteristics of the SmInZn, SmInCd, and SmTlZn compounds. The following important conclusions have been drawn from the calculations.

SmInZn, SmInCd, and SmTlZn are well stable in hexagonal phase.Equilibrium volume increases from SmInZn → SmTlZn → SmInCd due to increasing lattice parameter from SmInZn → SmTlZn → SmInCd. All three compounds confirm metallic nature due to dominancy of Sm-f spin up bands at the Fermi level. Sm-f spin up bands provide metallic character to these materials. Fermi energies E_F = 0.52524 electron-volts (eV) for SmInZn, E_F = 0.48818 electron-volts (eV) for SmInCd and E_F = 0.54729 electron-volts (eV) for SmTlZn.

Bulk modulus characteristics show that strength of SmInZn, SmInCd, and SmTlZn compounds decreases with temperature and become more flexible with increasing the temperature. The impact of temperature on Debye temperature, θ_D was found to be small on SmInZn and SmInCd while impact of temperature on θ_D is larger in SmTlZn. Thus, SmInZn was found to be stiffer than SmInZn and SmInCd. All three compounds show deviation from harmonic oscillator and SmInZn show larger deviation from harmonic oscillator character compared to SmInCd and SmTlZn. α increases with increasing the temperature due to expansion of unit cell dimensions and hence volume with temperature. The amount of disorder was found to be zero at 0K and increases rapidly with increasing the temperature in these compounds.

ORCID IDs

Aman Kumar, https://orcid.org/0000-0002-8867-6595; **Anuj Kumar**, https://orcid.org/0000-0003-3372-3718
Kamal Kumar, https://orcid.org/0000-0001-8132-5373

REFERENCES

[1] R.D. Hoffmann, and R. Pöttgen, Z. Kristallogr. **216**, 127 (2001).
[2] M.D. Klicpera, F. Malý, I. Puente-Orench, and P. Javorský, J. Alloys Compd. **822**, 153595 (2020). https://doi.org/10.1016/j.jallcom.2019.153595
[3] Mishra, U. Subbarao, S. Roy, S.C. Sarma, D. Mumaddi, S. Sarkar, and S.C. Peter, Inorg. Chem. **57**, 12576 (2018). https://doi.org/10.1021/acs.inorgchem.8b01650
[4] K. Sun, H. Yao, E. Fradkin, and S.A. Kivelson, Phys. Rev. Lett. **103**, 046811 (2009). https://doi.org/10.1103/PhysRevLett.103.046811
[5] L. Bessais, "Structure and Magnetic Properties of Intermetallic Rare-Earth-Transition-Metal Compounds: A Review", Materials, **15**, 201 (2022). https://doi.org/10.3390/ma15010201
[6] E. Burzo, "Exchange Interactions and Transition Metal Moments in Rare-Earth Compounds", J. Synchrotron Investig. **12**, 431 (2018). https://doi.org/10.1134/S1027451018030072
[7] M. Duchna, and I. Cieślik, "Rare Earth Elements in New Advanced Engineering Applications", Rare Earth Elements - Emerging Advances, Technology Utilization, and Resource Procurement, (2022). https://doi.org/10.5772/intechopen.109248
[8] M. Traore, A. Gong, Y. Wang, L. Qiu, Y. Bai, W. Zhao, Y. Liu, et al., "Research progress of rare earth separation methods and technologies", Journal of Rare Earths, (2022). https://doi.org/10.1016/j.jre.2022.04.009
[9] A. Fert, F.N. Van Dau, Comptes Rendus Physique, **20**(7-8), 817 (2019). https://doi.org/10.1016/j.crhy.2019.05.020
[10] V. Balaram, "Rare earth elements: A review of applications, occurrence, exploration, analysis, recycling, and environmental impact", Geoscience Frontiers, **10**(4), 1285 (2019). https://doi.org/10.1016/j.gsf.2018.12.005
[11] G. Barakos, H. Mischo, and J. Gutzmer, *A forward look into the US rare-earth industry; How potential mines can connect to the global REE market?,* Mining Engineering, (2018), pp. 30-37. https://thoriumenergyalliance.com/wp-content/uploads/2020/02/REE-GeorgeNabeelhighlights.pdf

[12] W. Gwenzi, L. Mangori, C. Danha, N. Chaukura, N. Dunjana, and E. Sanganyado, "Sources, behaviour, and environmental and human health risks of high-technology rare earth elements as emerging contaminants", The Science of the Total Environment, **636**, 299-313, (2018). https://doi.org/10.1016/j.scitotenv.2018.04.235
[13] J. Kang, and A.M. Kang, "Trend of the research on rare earth elements in environmental science", Environ. Sci. Pollut. Res. **27**, 14318 (2020). https://doi.org/10.1007/s11356-020-08138-z
[14] M.Y. Raïâ, R. Masrour, A. Jabar, M. Hamedoun, A. Rezzouk, A. Hourmatallah, N. Benzakour, et al., Journal of Physics and Chemistry of Solids, **163**, 110581 (2022). https://doi.org/10.1016/j.jpcs.2022.110581
[15] M. Jirsa, M. Rameš, and M. Muralidhar, Acta Phys. Pol. A, **113**, 223 (2008). http://przyrbwn.icm.edu.pl/APP/PDF/113/a113z1054.pdf
[16] D.J. García, V. Vildosola, and P. Cornaglia, Condensed Matter, **32**(28), 285803 (2019). https://doi.org/10.1088/1361-648X/ab7e5a
[17] X.B. Liu, and Z. Altounian, "First-principles calculation on the Curie temperature of GdFeSi", J. Appl. Phys. **107**, 09E103 (2010). https://doi.org/10.1063/1.3364048
[18] S. Talakesh, and Z. Nourbakhsh, "The density functional study of structural, electronic, magnetic and Thermodynamic properties of XFeSi (X=Gd, Tb, La) and GdRuSi compounds", J. Supercond. Novel Magn. **30**, 2143 (2017). https://doi.org/10.1007/s10948-017-3976-x
[19] V.K. Pecharsky, and K.A. Gschneidner Jr, "Magnetocaloric effect and magnetic refrigeration", J. Magn. Magn. Mater. **44-56**, 200 (1999). https://doi.org/10.1016/S0304-8853(99)00397-2
[20] J. Du, Q. Zheng, Y. Li, Q. Zhang, D. Li, and Z. Zhang, "Large magnetocaloric effect and enhanced magnetic refrigeration in ternary Gd-based bulk metallic glasses", J. Appl. Phys. **103**, 023918 (2008). https://doi.org/10.1063/1.2836956
[21] V. Franco, J.S. Blázquez, J.J. Ipus, J.Y. Law, L.M. Moreno-Ramírez, and A. Conde, Prog. Mater. Sci. **93**, 112 (2018). https://doi.org/10.1016/j.pmatsci.2017.10.005
[22] A. Mahmood, M. Rashid, K. Safder, M.W. Iqbal, N.A. Noor, S.M. Ramay, W. Al-Masry, et al., Results in Physics, **20**, 103709 (2021). https://doi.org/10.1016/j.rinp.2020.103709
[23] P. Blaha, K. Schwarz, G.K.H. Madsen, D. Kuasnicka, and J. Luitz, *WIEN2k An Augmented Plane Wave-Local Orbitals Program for Calculating Crystal Properties*, (K. Schwarz Technical Universitat, Wien Austria, 2001). ISBN: 3-9501031 1-2
[24] D.J. Singh, and L. Nordstrom, *Plane Waves Pseudo Potentials and the LAPW Method*, (Springer, New York, 2006).
[25] K. Schwarz, "DFT calculations of solids with LAPW and WIEN2k", J. Solid State Chemistry, **176**, 319 (2003). https://doi.org/10.1016/S0022-4596(03)00213-5
[26] A. Otero-de-la-Roza, and, D. Abbasi-Pérez, and V. Luaña, "GIBBS2: A new version of the quasiharmonic model code. II. Models for solid-state thermodynamics, features, and implementation", Computer Physics Communications, **182**. 2232 (2011). https://doi.org/10.1016/j.cpc.2011.05.009
[27] W. Kohn, and L.J. Sham, Phys. Rev. **140**, A1133 (1965). https://doi.org/10.1103/PhysRev.140.A1133
[28] P. Blaha, K. Schwarz, G.K.H. Madsen, D. Kvasnicka, and J. Luitz, *WIEN2k, An Augmented Plane Wave Plus Local Orbital Program for Calculating Crystal Properties*, (Vienna University of Technology, Vienna, 2001).
[29] J.P. Perdew, K. Burke, and M. Ernzerhof, Phys. Rev. Lett. **77**, 3865 (1996). https://doi.org/10.1103/PhysRevLett.77.3865
[30] F.D. Murnaghan, Proc. Natl. Acad. Sci. U.S.A. **30**, 244 (1994). https://doi.org/10.1073%2Fpnas.30.9.244
[31] K. Hartjes, and W. Jeitschko, J. Alloys Compd. **226**, 81 (1995). https://doi.org/10.1016/0925-8388(95)01573-6

ЕЛЕКТРОННІ ТА ТЕРМОДИНАМІЧНІ ВЛАСТИВОСТІ ПОТРІЙНИХ РІДКІСНОЗЕМЕЛЬНИХ СПЛАВІВ

Аман Кумар[a], Анудж Кумар[b], Камал Кумар[c], Ріші Пал Сінгх[d], Ріту Сінгх[e], Раджеш Кумар[f]
[a]Факультет фізики, Науковий коледж Керала Верми Субхарті, Університет Свамі Вівекананда Субхарті, Мірут, Уттар-Прадеш, Індія
[b]Факультет фізики, Махамайя Державний коледж, Шеркот, Бійнор, Уттар-Прадеш, Індія
[c]Факультет фізики, D.A.V College Kanpur, Уттар-Прадеш, Індія
[d]Факультет фізики, S. S. V. College, Хапур 245101, Уттар-Прадеш, Індія
[e]Факультет хімії, S. S. V. Коледж, Хапур 245101, Уттар-Прадеш, Індія
[f]Факультет фізики, Державний коледж, Нанаута, Сахаранпур, Уттар-Прадеш, Pin-247452, Індія

У цій статті використовується підхід FP-LAPW в рамках методу DFT і квазігармонійна модель Дебая для дослідження електронних і термодинамічних властивостей інтерметалічних рідкоземельних матеріалів таких як SmInZn, SmInCd і SmTlZn. Термодинамічні властивості були визначені за допомогою квазігармонічної моделі Дебая, тоді як підходи FP-LAPW в рамках методу DFT були використані для отримання електронних властивостей. Розраховані структурні параметри та наявні експериментальні дані були досліджені, і було помічено, що існує хороша узгодженість між доступними експериментальними та розрахунковими значеннями структурних параметрів. Електронна поведінка сполук SmInZn, SmInCd та SmTlZn демонструє металевий характер. Ми розглянули кілька термодинамічних характеристик. Усі розраховані характеристики збігаються з експериментальними або теоретичними розрахунками.

Ключові слова: *електроніка; інтерметаліди; щільність стану; DFT*